A *Gja1* missense mutation in a mouse model of oculodentodigital dysplasia

Ann M. Flenniken[1,*], Lucy R. Osborne[1,2,3,*], Nicole Anderson[4], Nadia Ciliberti[5], Craig Fleming[1], Joanne E. I. Gittens[6], Xiang-Qun Gong[6], Lois B. Kelsey[1], Crystal Lounsbury[7], Luisa Moreno[8], Brian J. Nieman[9,10], Katie Peterson[1], Dawei Qu[8], Wendi Roscoe[7], Qing Shao[7], Dan Tong[6], Gregory I. L. Veitch[6,7], Irina Voronina[1], Igor Vukobradovic[1], Geoffrey A. Wood[1], Yonghong Zhu[11], Ralph A. Zirngibl[3], Jane E. Aubin[1,3], Donglin Bai[6], Benoit G. Bruneau[3,11,12], Marc Grynpas[1,13], Janet E. Henderson[14], R. Mark Henkelman[9,10], Colin McKerlie[1,13,15], John G. Sled[9,10], William L. Stanford[1,4,5], Dale W. Laird[6,7], Gerald M. Kidder[6], S. Lee Adamson[1,12,16] and Janet Rossant[1,3,†]

[1]Centre For Modeling Human Disease, Samuel Lunenfeld Research Institute, Mount Sinai Hospital, 600 University Avenue, Toronto, Ontario M5G 1X5, Canada
[2]Department of Medicine, Medical Sciences Building, 1 King's College Circle, University of Toronto, Toronto, Ontario M5S 1A8, Canada
[3]Department of Molecular and Medical Genetics, Medical Sciences Building, 1 King's College Circle, University of Toronto, Toronto, Ontario M5S 1A8, Canada
[4]Institute of Medical Science, University of Toronto, Toronto, Ontario M5S 1A8, Canada
[5]Institute of Biomaterials and Biomedical Engineering, University of Toronto, Toronto, Ontario M5G 1X8, Canada
[6]Department of Physiology and Pharmacology, University of Western Ontario, Dental Science Building, London, Ontario N6A 5C1, Canada
[7]Department of Anatomy and Cell Biology, University of Western Ontario, Dental Science Building, London, Ontario N6A 5C1, Canada
[8]Samuel Lunenfeld Research Institute, Mount Sinai Hospital, Toronto, Ontario M5G 1X8, Canada
[9]Mouse Imaging Centre, The Hospital for Sick Children, 555 University Avenue Toronto, Ontario M5G 1X8, Canada
[10]Department of Medical Biophysics, University of Toronto, Toronto, Ontario M5S 1A8, Canada
[11]Cardiovascular Research, The Hospital for Sick Children, Toronto, Ontario M5S 1A8, Canada
[12]Heart and Stroke/Richard Lewar Centre of Excellence, University of Toronto, Toronto, Ontario M5S 1A8, Canada
[13]Department of Laboratory Medicine and Pathobiology, University of Toronto, Toronto, Ontario M5S 1A8, Canada
[14]Department of Medicine and Centre for Bone and Periodontal Research, McGill University, 740 Avenue Dr Penfield, Montreal, Quebec H3A 1A4, Canada
[15]Integrative Biology Research Program, The Hospital for Sick Children, Toronto, Ontario M5S 1A8, Canada
[16]Department of Obstetrics and Gynecology, University of Toronto, Toronto, Ontario M5S 1A8, Canada

*These authors contributed equally to this work
†Author for correspondence (e-mail: rossant@mshri.on.ca)

Summary

Oculodentodigital dysplasia (ODDD) is an autosomal dominant disorder characterized by pleiotropic developmental anomalies of the limbs, teeth, face and eyes that was shown recently to be caused by mutations in the gap junction protein alpha 1 gene (*GJA1*), encoding connexin 43 (Cx43). In the course of performing an N-ethyl-N-nitrosourea mutagenesis screen, we identified a dominant mouse mutation that exhibits many classic symptoms of ODDD, including syndactyly, enamel hypoplasia, craniofacial anomalies and cardiac dysfunction. Positional cloning revealed that these mice carry a point mutation in *Gja1* leading to the substitution of a highly conserved amino acid (G60S) in Cx43. In vivo and in vitro studies revealed that the mutant Cx43 protein acts in a dominant-negative fashion to disrupt gap junction assembly and function. In addition to the classic features of ODDD, these mutant mice also showed decreased bone mass and mechanical strength, as well as altered hematopoietic stem cell and progenitor populations. Thus, these mice represent an experimental model with which to explore the clinical manifestations of ODDD and to evaluate potential intervention strategies.

Key words: Oculodentodigital dysplasia, Connexin 43, Missense mutation, Mouse model

Introduction

Oculodentodigital dysplasia (ODDD) is an autosomal dominant disorder characterized by pleiotropic developmental anomalies of the limbs, teeth, face and eyes (Loddenkemper et al., 2002; Paznekas et al., 2003). Common symptoms comprise syndactyly of the hand and foot; microdontia and enamel hypoplasia; craniofacial alterations, including a depressed nasal bridge with a long narrow nose and microcephaly; and

ophthalmic alterations, such as microphthalmia, cataracts and abnormalities of the iris (Loddenkemper et al., 2002; Paznekas et al., 2003). Additional symptoms with variable penetrance have been described in individuals with ODDD, including cardiac arrhythmias, hearing loss and neurological disorders such as weakness of the lower extremities and an abnormal gait (Loddenkemper et al., 2002; Paznekas et al., 2003).

Recently, mutations in the gap junction protein alpha 1 gene (*GJA1*) encoding connexin 43 (Cx43) have been found in families with ODDD (Paznekas et al., 2003). In humans, Cx43 belongs to a large family of 21 proteins whose structure consists of an intracellular N terminus, four transmembrane domains with one intracellular loop and two extracellular loops, ending with an intracellular C terminus. Six connexin proteins form a ring with a central pore, collectively known as a connexon or hemichannel. An intercellular gap junction or channel is formed when a hemichannel from one cell docks with a hemichannel from an apposing cell. Gap junctions provide an intercellular pathway for the passage of small ions and molecules involved in cell to cell communication that are integral to many developmental and physiological processes (Sohl and Willecke, 2004). Mutations in human *GJA1* are predicted to perturb the formation of functional gap junctions. To date, there are 27 reported mutations in the *GJA1* gene that are linked to ODDD but, in most cases, the mechanism of action of these mutations remains unclear (Kjaer et al., 2004; Paznekas et al., 2003; Richardson et al., 2004; van Steensel et al., 2005; Vitiello et al., 2005). Recently, it was shown that the G21R and G138R mutations result in loss-of-function Cx43 and these mutants have dominant properties on wild-type Cx43 (Roscoe et al., 2005). In these studies, however, the mutants were expressed in excess of wild type Cx43 leading to concerns that this did not adequately represent the human disease condition.

In the course of performing an N-ethyl-N-nitrosourea (ENU) mutagenesis screen in mice, we identified a dominant mutation that exhibits many classic symptoms of ODDD, including syndactyly, enamel hypoplasia, craniofacial anomalies and cardiac dysfunction. Positional cloning revealed that these mice carry a point mutation in *Gja1*, leading to the substitution of a highly conserved amino acid (G60S) in Cx43. The availability of this mouse model system allowed us to undertake a histological and functional analysis of gap junctions in order to determine their role in the ODDD phenotype. Interestingly, we found a dramatic reduction in total Cx43 protein, in gap junctional intercellular coupling and in the number of gap junction plaques, indicating that this mutation is not simply a loss-of-function mutation but rather a dominant-negative mutation. In addition, we have found alterations in bone properties and in the hematopoietic system that have not yet been reported for individuals with ODDD but which are consistent with the known importance of gap junction function in these tissues.

Materials and methods

Mice and ENU mutagenesis

C57BL/6J (B6) males, C3H/HeJ (C3) males/females and FVB females were purchased from the Jackson Laboratory at 6-8 weeks of age. Male C57BL/6J mice received three intraperitoneal injections of ENU, 1 week apart, at a dose of 85 mg/kg as described previously

(Justice et al., 2000). ENU mutagenized males were bred to C3H/HeJ females and the offspring produced from these matings were C3;B6 F1 hybrid pups, known as Generation1 (G1). G1 mice were screened for traits of interest, bred to C3H/HeJ mice, and the G2s (C3;CgN2) produced were tested for heritability and used for genetic mapping. Lines were maintained by breeding to C3H/HeJ mice producing G3(C3;CgN3) and G4(C3;CgN4) mice. To produce a larger mouse, capable of carrying the telemetry implant, the G3 mice were bred to FVB females to produce FVB;C3 F1 (FVB;C3CgN3) mice. Mice carrying the *Gja1^{Jrt}* mutation bred onto the C3 background are referred to as *Gja1^{Jrt}/+* and on the FVB and C3 mixed background as *Gja1^{Jrt}/+ × FVB*. All experimental procedures received approval from the local Animal Care Committee and were conducted in accordance with the guidelines of the Canadian Council on Animal Care.

Genetic mapping

DNA was extracted from tail tissue using standard procedures followed by PCR amplification of individual microsatellite markers using fluorescently tagged primers (IDT, Coralville, IA). Cycles were performed as follows: 94°C for 3 minutes; 35 cycles of 94°C for 30 seconds, 55°C for 30 seconds and 72°C for 30 seconds; and a final extension of 72°C for 5 minutes. The labeled products were then multiplexed and analyzed on a BaseStation automated sequencer (MJ Research, Waltham, MA) to determine whether, for any given marker, an allele from the mutagenized strain (C57BL/6J) had been inherited.

In-life screening of mutants

The appearance and behavior screening was performed using a modified SHIRPA protocol (Rogers et al., 1997) with details at www.CMHD.ca We used a 20 kHz Clickbox (MRC Institute of Hearing, Nottingham, UK) to elicit the Preyer reflex indicative of normal hearing. Eyes were scanned for abnormalities using a pen light to reveal opacities and to assess pupillary light reflex. Extended observation and handling was used to detect gait abnormalities and/or limb weakness.

Pathology

Mice were sacrificed using a combination of CO_2 and O_2 and tissues collected and fixed in 10% neutral buffered formalin or Bouin's fixative. Tissue sections (4 μm) were prepared and stained with Hematoxylin and Eosin.

Limb and tooth analysis

External images of the limbs and teeth were taken using a Sony DSC-S50 Cyber-shot digital camera. X-ray imaging was performed using a Faxitron Specimen Radiography System, Model MX-20. Freshly dissected teeth from an 11-week-old *Gja1^{Jrt}/+* mouse and unaffected littermate were embedded in epoxy. By use of a Buehler grinder/polisher, teeth were ground and polished with 1 μm diamond grit in sagittal section. Imaging was performed on an FEI XL-30 scanning electron microscope at 20 kV with a back-scatter detector.

MRI and micro-CT

Five *Gja1^{Jrt}/+* mice and five control mice (ranging in age from 52 to 60 weeks of age) were analyzed using a 7 Tesla MRI (Varian Instruments, Pala Alto, CA) modified for parallel imaging. T2-weighted 3D datasets with 120 μm resolution were acquired (Nieman et al., 2004) and reviewed visually for intensity differences. Following MRI, the animals were sacrificed, perfused with formalin and decapitated in preparation for scanning using a micro-computed tomography unit (GE Medical Systems, London, ON). The resulting 60 μm resolution 3D datasets were used to assess differences in skull shape between animals using an automated technique for detecting shape differences based on estimating the non-linear deformation needed to bring individual images into alignment (Kovacevic et al., 2005). The deformation representing the between-group shape

differences was assessed by a Hotelling T^2 test (Gaser et al., 1999) with overall significance established by permutation testing (Holmes et al., 1996).

Analyses of the heart

Results are presented as mean±s.e.m. for n (number of mice). Unpaired t-tests were performed for group comparisons.

Ultrasound

The rectal temperature of isoflurane-anesthetized mice was maintained at 36-38°C and the heart rate was monitored via transcutaneous electrodes (ECG/heat Pad; Indus Instruments, Houston TX). A 20 MHz transcutaneous pulsed Doppler instrument was used to measure the blood velocity in the ascending aorta of five $Gja1^{Jrt}$/+ mice and five wild-type littermates at 11-14 weeks, and nine $Gja1^{Jrt}$/+ mice and seven controls at 50-67 weeks. Peak velocity, acceleration, pre-ejection time, ejection time and stroke distance were measured from a representative waveform in a 3 second file (DSPW; Indus Instruments). The same Doppler instrument and the same mice were used to obtain the blood velocity waveform in the left ventricular (LV) chamber. Peak E, peak A, isovolumetric relaxation (IVRT) and contraction (IVCT) times, and ejection time (ET) were measured and the Myocardial Performance Index (MPI) calculated ((IVRT + IVCT)/ET) (Broberg et al., 2003). A 30 MHz ultrasound biomicroscope (Vevo 660; VisualSonics, Toronto, Canada) was used to perform an echocardiographic exam on five $Gja1^{Jrt}$/+ mice and five wild-type littermates at 8-11 weeks, and four $Gja1^{Jrt}$/+ mice and three controls at 50-67 weeks, using published methods (Zhou et al., 2004). LV and right ventricular (RV) inner chamber dimensions (ID) and wall thicknesses (WT) at end-systole and end-diastole were measured and fractional shortening (FS) [(ID$_d$–ID$_s$)/ID$_d$ × 100] and relative wall thickness (wall thickness/inner dimension) were calculated. Aortic and pulmonary artery diameters and peak blood velocities, and right atrial chamber dimension were also measured. Dimension $\propto$ weight$^{0.33}$ was used to correct dimension and diameter measurements for body size. The same ultrasound tests were also performed on five $Gja1^{Jrt}$/+ × FVB mice and five wild-type littermates at 7 weeks of age.

Acute ECG

A 1-minute recording of ECG was obtained acutely from nine isoflurane-anesthetized $Gja1^{Jrt}$/+ mice and eight controls at 50-67 weeks using subcutaneous pin electrodes, while rectal temperature was maintained at 36-38°C. Heart rate, P duration, PR interval, QRS duration and QTmax were measured from a signal-averaged ECG waveform obtained from a relatively noise-free section of the file (averaged over ~130 cycles; SAECG Chart 4, ADInstruments).

Chronic ECG by radio-telemetry

ECG telemetry devices (DSI) were implanted subcutaneously under anesthesia in nine $Gja1^{Jrt}$/+ × FVB mice and seven wild-type littermates at 11-13 weeks of age. Mice were allowed to recover for 72 hours before obtaining a continuous 48 hour recording. Measurements (P wave height and width, PQ interval, QRS width, QT interval, heart rate) were made from 20 ECG waveforms obtained over 24 hours and averaged for each animal. Entire 48 hour recordings were examined manually by a trained observer blind to genotype for sporadic events.

Micro-CT of femurs and vertebrae

The distal metaphysis of the left femurs and 4th lumbar vertebrae were scanned with a Skyscan 1072 micro-CT instrument (Skyscan, Belgium) at the Centre for Bone and Periodontal Research (www.bone.mcgill.ca) as described (Valverde-Franco et al., 2004). Two-dimensional images were used to generate 3D reconstructions of the bones from four $Gja1^{Jrt}$/+ mice and four wild-type littermates, ranging in age from 6-12 weeks. Morphometric parameters, including percent bone, trabecular thickness distribution, trabecular connectivity, structure model index and cortical thickness, were calculated with 3D Creator software supplied with the instrument.

Bone mineral density

Dual energy x-ray absorptiometry (PIXImus, Lunar Corp., Madison, WI) was used to measure bone mineral content (BMC), bone area and bone mineral density (BMD) of femurs in five $Gja1^{Jrt}$/+ × FVB mice and six wild-type littermates (22-week-old males).

Mechanical testing

Destructive three-point bending was performed on femurs of five $Gja1^{Jrt}$/+ × FVB mice and six wild-type littermates (22-week-old males) using a screw-driven mechanical testing machine (Instron model 1011, Canton, MA). Each bone was placed on two supports spaced 6.0 mm apart, and a load was applied to the bone midway between the supports at a deformation rate of 1 mm/minute. From the load displacement curve, the maximum load (ultimate load) and maximum displacement (failure displacement) were measured, and the stiffness was determined from a linear regression of the initial region of the curve. The toughness was determined by measuring the area under the load deformation curve.

Whole-mount Alcian Blue-Alizarin Red staining

Three- and 8-day-old $Gja1^{Jrt}$/+ mice and wild-type littermates were stained with Alcian Blue-Alizarin Red S as described previously (McLeod, 1980).

Hematopoietic analyses

Flow cytometric analysis of bone marrow, splenic and thymocyte subpopulations was performed on four $Gja1^{Jrt}$/+ mice and four controls (15-18 weeks), and two $Gja1^{Jrt}$/+ mice and two controls (57-62 weeks) using standard procedures and a panel of commercially available antibodies (anti-CD3ϵ, anti-CD4, anti-CD8, anti-CD11b, anti-CD41, anti-CD61, anti-B220, anti-Ly6G, and anti-TER-119; BD PharMingen, San Diego, CA) as previously described (Ito et al., 2003). The appropriate conjugated rat anti-mouse mAbs were used as negative controls. Side population analysis by Hoechst dye (Sigma H-6024) exclusion was performed on two $Gja1^{Jrt}$/+ mice and two controls (15 weeks), and two $Gja1^{Jrt}$/+ mice and two controls (57-62 weeks) according to published protocols by the Goodell laboratory and posted online (http://www.bcm.edu/genetherapy/goodell/new_site/index2.html). Flow cytometry was performed using a MoFlow cell sorter (Dako-Cytomation). Clonogenic assays were performed using commercially available methylcellulose containing IL3, IL6, SLF, and EPO (M3434, Stem Cell Technologies, Vancouver, BC) as previously described (Ito et al., 2003). Colony forming units-erythroid (CFU-E) were assayed after 2 days by staining in situ with benzidine (Sigma) to detect hemoglobin. BFU-E (burst forming units-erythroid) and CFU-C (CFU-GEMM, colony forming units-granulocyte, erythroid, macrophage, megakaryocyte; CFU-GM, colony forming units-granulocyte, macrophage; CFU-M, colony forming units-macrophage; CFU-G, colony forming units-granulocyte) were counted after 7-10 days by colony morphology.

Analysis of gap junctions and intercellular coupling among mutant granulosa cells

Paraffin sections were prepared from Bouin's-fixed ovaries as described (Roscoe et al., 2001). They were immunostained using an affinity purified rabbit polyclonal antibody raised against residues 360-382 of rat Cx43 (Mitchell et al., 2003) and Alexa Fluor-conjugated goat anti-rabbit IgG (Molecular Probes). The final wash contained Hoechst 33342 (Molecular Probes) to stain nuclei.

Preantral follicles were isolated from ovaries of $Gja1^{Jrt}$/+ females and wild-type littermates at 6-8 weeks and from $Gja1^{Jrt}$/+ × FVB females and wild-type littermates at 12 weeks and cultured on cover

slips in modified Waymouth MB 752/1 medium for dye transfer experiments as previously described (Gittens et al., 2003). Granulosa cells were microinjected with 5% Lucifer yellow (Sigma-Aldrich) in double distilled H_2O. Images were captured 2 minutes after injection and the number of cells receiving dye was scored. Some follicles were fixed in 80% methanol/20% acetone for 15 minutes at 4°C for Cx43 immunostaining as described above.

For conductance measurements, granulosa cells were constantly perfused with a solution containing (mM) NaCl (140.0), KCl (5.4), $MgCl_2$ (1.0), $CaCl_2$ (1.8), and HEPES (10.0) (pH 7.4). Whole-cell voltage clamp (V_H –60 mV) was applied to a single granulosa cell at room temperature. Current signals, low-pass filtered at 10 kHz, were recorded using an Axopatch 200B amplifier and digitized at 100 kHz sampling rate. The resulting capacitative current transient was analyzed to obtain the peak current I_p and the steady-state current I_{ss}. The gap junctional conductance between the patched cell and the surrounding rings of cells (G_{01x}) was calculated according to the equation $G_{01x}=I_{ss}*G_{ser}/(I_p-I_{ss})$, where G_{ser} is the series conductance ($G_{ser}=I_p/10$ mV) (de Roos et al., 1996). The resistance of the patch pipette was 2-4 MΩ when filled with a solution containing (mM) KCl (130.0), NaCl (10.0), EGTA (2.0), $MgCl_2$ (4.0), HEPES (10.0) and TEA (5.0), pH 7.3.

Western blot analysis

Heart and ovaries were collected from $Gja1^{Jrt}$/+ mice and wild-type littermates (11 weeks, and 29-34 weeks), homogenized and subjected to cell lysis as described (Thomas et al., 2004). Total protein (30 μg) was loaded into each lane and subjected to SDS-PAGE. Western blots were performed using rabbit anti-Cx43 polyclonal (Sigma) and mouse anti-GAPDH monoclonal antibodies as described (Thomas et al., 2004).

Analysis of Cx43[G60S] localization and function in transfected cell lines

The Cx43[G60S] mutation (G to A at position 177) was constructed using the Quick-Change Site Directed Mutagenesis Kit (Stratagene, La Jolla, California) as directed. The wild-type and mutant cDNAs were fused with a GFP tag at the C terminus and cloned into the pEGFP-N1 vector (BD Biosciences, Clontech, La Jolla, California). Normal rat kidney (NRK), mouse neuroblastoma (N2A) and human cervical carcinoma (HeLa) cells were transfected and immunolabeled using established procedures (Laird et al., 1995; Roscoe et al., 2005; Thomas et al., 2004). Dual patch clamp recording was used to measure gap junctional coupling between pairs of transfected N2A cells as previously described (Roscoe et al., 2005).

Results

A *Gja1* missense mutation results in mice with morphological characteristics of ODDD

A dominant screen in offspring of ENU mutagenized C57BL/6J male mice crossed with C3H/HeJ females identified a mutant line ($Gja1^{Jrt}$) with fully penetrant, but variable fusion of digits 2, 3 and 4 on all limbs (Fig. 1A,C). Faxitron analysis revealed fusion of soft tissue but not bone (Fig. 1B,D). The $Gja1^{Jrt}$/+ mice
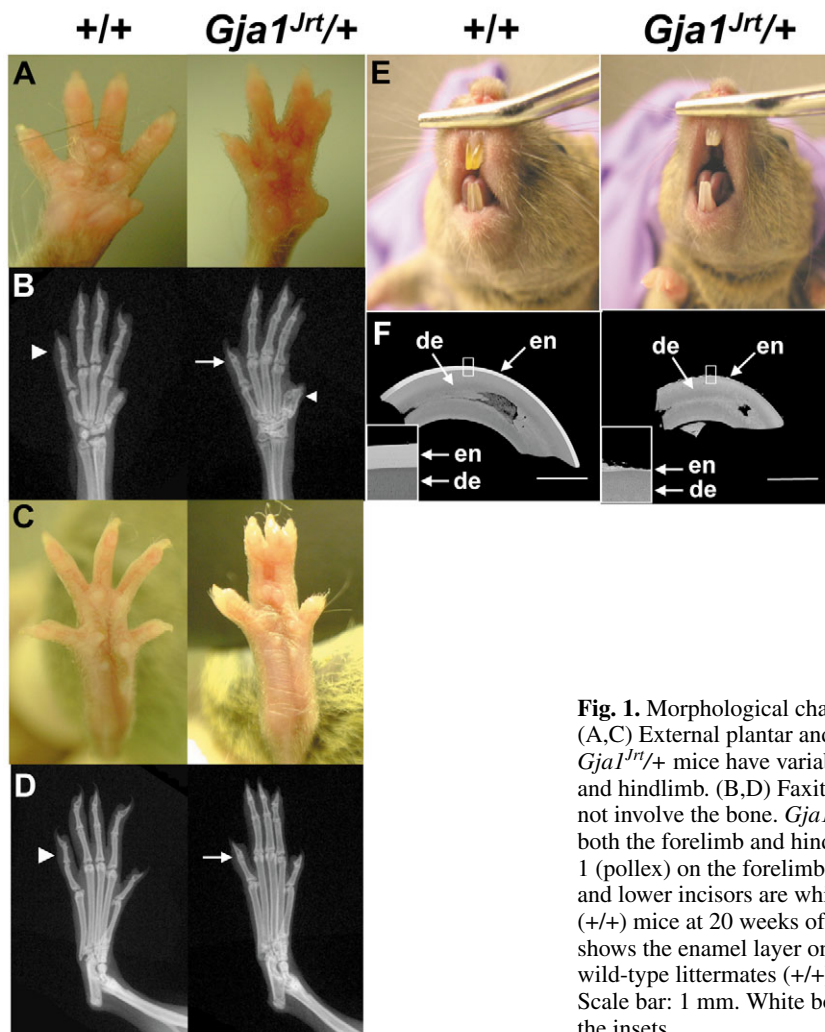

Fig. 1. Morphological characteristics of mice heterozygous for the $Gja1^{Jrt}$ mutation. (A,C) External plantar and x-ray images taken at 11 weeks of age show that $Gja1^{Jrt}$/+ mice have variable soft tissue fusion of digits 2, 3 and 4 on the forelimb and hindlimb. (B,D) Faxitron analysis shows the digit fusion in $Gja1^{Jrt}$/+ mice does not involve the bone. $Gja1^{Jrt}$/+ are missing the middle phalange of the last digit on both the forelimb and hindlimb (arrows) and exhibit abnormal bone growth of digit 1 (pollex) on the forelimb (arrowhead). (E) Upper incisors are small and both upper and lower incisors are white in the $Gja1^{Jrt}$/+ mice, instead of yellow as in wild-type (+/+) mice at 20 weeks of age. (F) Back-scatter scanning electron microscopy shows the enamel layer on $Gja1^{Jrt}$/+ upper incisors is very thin compared with wild-type littermates (+/+), and is nearly absent in places. de, dentine; en, enamel. Scale bar: 1 mm. White boxes indicate the area of higher magnification as seen in the insets.

were visibly smaller than their wild-type littermates at all ages and on both genetic backgrounds examined (C3;B6 and FVB × C3;B6). The causative mutation was mapped to a 55 Mb interval of mouse chromosome 10 bounded by *D10Mit3* and *D10Mit42* (see Fig. S1A in the supplementary material) that is syntenic to human chromosomes 6q21-q23 and 10q21-q22. Two disorders with a syndactyly phenotype map to 6q22: type III Syndactyly (OMIM 186100) and ODDD (OMIM 164200) (www.ncbi.nlm.nih.gov/entrez/query.fcgi?db=OMIM). ODDD has recently been shown to result from point mutations in *GJA1* encoding Cx43 (Paznekas et al., 2003). Genomic sequencing of the mutant line revealed a point mutation in *Gja1* that changed a highly conserved glycine to a serine at residue 60 in the first extracellular loop of Cx43 (see Fig. S1B in the supplementary material). This substitution was not found in either parental strain.

Limb and dental characteristics of *Gja1^Jrt^/+* mutant mice

The phenotype of our syndactyly mutant showed striking similarities to that of individuals with ODDD. As well as simple fusion of the digits, the middle phalange on the last digit of both the forelimb and hindlimb was absent (Fig. 1B,D) which is consistent with ODDD (Loddenkemper et al., 2002; Paznekas et al., 2003). In addition, digit 1 (pollex) on the forelimb consisted of a thickened, malformed bone that resulted possibly from abnormal growth or a fusion of the phalanges (Fig. 1B). Mutant mice had small, white upper and lower incisors that were prone to breakage, instead of the normal yellow, enamel covered teeth (Fig. 1E). Further analysis by back-scatter scanning electron microscopy revealed a very thin, porous enamel layer that was almost non-existent in some areas (Fig. 1F). The majority of individuals with ODDD also have abnormal dentition, with enamel hypoplasia, microdontia, multiple caries and early tooth loss (Loddenkemper et al., 2002; Paznekas et al., 2003).

Craniofacial and ocular anomalies of *Gja1^Jrt^/+* mutant mice

Craniofacial and ocular anomalies are also common in ODDD, with many individuals exhibiting a long, narrow nose, depressed nasal bridge and microcephaly, as well as small

sunken eyes, cataracts, glaucoma and malformations of the iris (Loddenkemper et al., 2002; Paznekas et al., 2003). Analysis by micro-computed tomography (micro-CT) yielded a surface rendering representative of an average skull of five *Gja1^Jrt^/+* and five wild-type mice (Fig. 2) ranging in age from 54 to 60 weeks. Average skull shapes were overlaid and the magnitude of the deformation needed to map the control skull (+/+) onto the average *Gja1^Jrt^/+* skull was calculated. After removing linear differences in overall skull size, orientation and skew, significant shape alterations were observed, including depression across the bridge of the nose and eye sockets, and an outward displacement of the frontal and occipital bones of the skull (Fig. 2). We observed corneal opacity in four out of 16 mutant mice examined (5-34 weeks of age) and a subset of these mice (2/4) also had apparent iris malformations as evidenced by abnormal pupil shape and pupillary light reflex. None of the 25 control mice of similar age range showed any eye abnormalities.

Cardiac disturbances in *Gja1^Jrt^/+* and FVB × *Gja1^Jrt^/+* mutant mice

Documented heart dysfunction in ODDD includes atrioseptal defects and arrhythmias such as ventricular tachycardia and atrioventricular (AV) block (Loddenkemper et al., 2002; Paznekas et al., 2003). *Gja1^Jrt^/+* mice also exhibited abnormalities in heart morphology and electrophysiological function. Immunofluorescence showed a pronounced reduction in myocardial gap junctions (Fig. 3A,B) and a patent foramen ovale was observed in two out of five mutants examined (Fig. 3C,D). Small, multifocal lesions of myocardial mineralization, mild fibrosis and inflammation were also observed in *Gja1^Jrt^/+* mutants but not controls (see Fig. S4 in the supplementary material and data not shown). Two out of nine mutants exhibited highly abnormal cardiac conduction and/or contraction defects: the QRS duration was prolonged and premature ventricular contractions (ectopic beats) occurred during the 1-minute ECG recording session in one mutant; in the other, the PR interval was prolonged and the 'myocardial performance index' was elevated (Broberg et al., 2003), suggesting poor global cardiac function. Variables were more than two standard deviations from the mean of the controls, although group means for these variables were not significantly affected. As a group, older
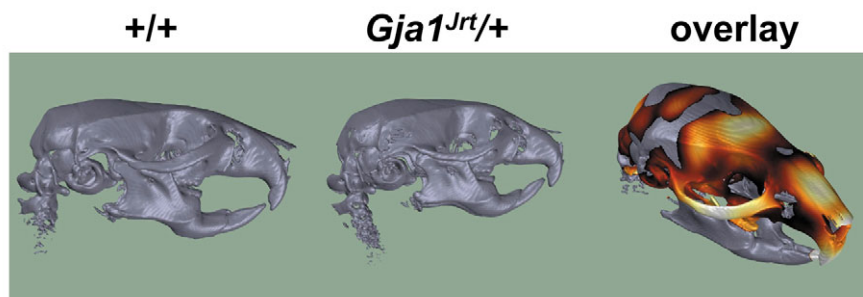

Fig. 2. Micro-computed tomography of *Gja1^Jrt^/+* skulls. Surface renderings of average skulls in orthographic projection were constructed from five *Gja1^Jrt^/+* mice and five control mice (+/+) ranging in age from 54-60 weeks of age. There are differences seen in profiles along the dorsal surface of the skull. Average skull shapes were overlaid with the magnitude of the deformation needed to map the control skull (+/+) onto the average *Gja1^Jrt^/+* skull. The false color range (indicative of deformation) is from 120 μm (black) to 720 μm (white). Colored regions were statistically significant ($P<0.01$) by a Hotelling T^2 statistic comparing the two groups. There is a large deformation across the bridge of the nose depressing the nasal bone and eye sockets by 668±218 μm and 760±150 μm, respectively, as well as the outward displacement of the frontal bone and occipital bone of 680±265 μm and 460±269 μm, respectively.
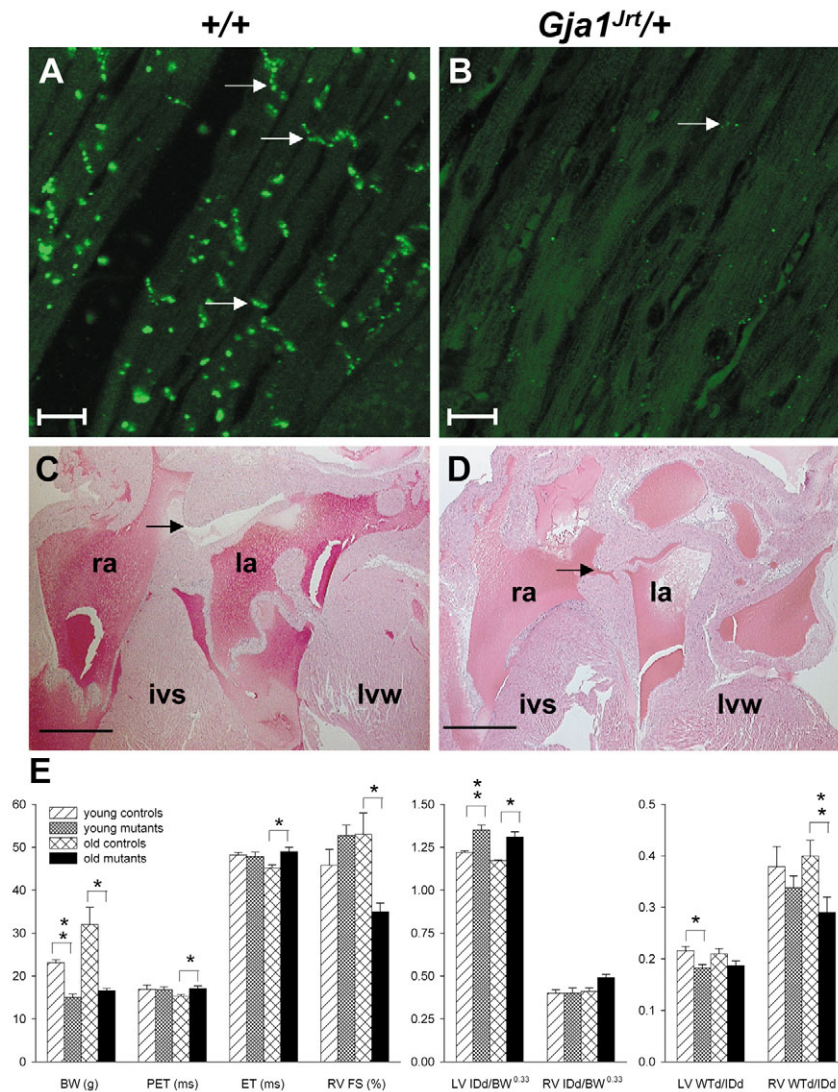
+/+   Gja1^{Jrt}/+

Fig. 3. Cardiac phenotype of $Gja1^{Jrt}$/+ mutants. Histopathology revealed very few, tiny 'gap junctions' in the longitudinal muscle fibers of the myocardium of mutants following immunofluorescence for Cx43 (green) (arrow) compared with wild-type controls (+/+) in which intense Cx43 staining is seen in the gap junctions at the intercalated disks (arrows) (A,B). Histopathology also revealed patent foramen ovale in some mutants (arrows in C,D). The body weight (BW) of $Gja1^{Jrt}$/+ mutants was markedly reduced relative to controls both when young (8-14 weeks) and when old (50-67 weeks) (E). The left ventricular inner chamber dimension in diastole (LV IDd) was large relative to the body weight$^{0.33}$ and the ventricular wall thickness in diastole (WTd) was reduced relative to the LV IDd in $Gja1^{Jrt}$/+ mutants (E). In older mutants, there was a prolongation of the LV pre-ejection time (PET) and ejection time (ET) when compared with controls (E). Old mutants evaluated by echocardiography exhibited reduced right ventricular (RV) fractional shortening (FS) and reduced RV WTd, suggesting the development of RV failure with aging (E). LV FS did not change (not shown). *P<0.05, **P≤0.005. Scale bars: 20 μm in A,B; 500 μm in C,D. la, left atrium; ra, right atrium; lvw, left ventricular wall; ivs, interventricular septum.

mutants (50-67 weeks) exhibited significantly reduced right ventricular fractional shortening and diastolic wall thickness (expressed relative to chamber dimension), suggesting the development of right ventricular failure with aging (Fig. 3E). Left ventricular structure and function were also significantly affected in mutants; pre-ejection and ejection times were elevated, diastolic chamber dimension (expressed relative to body weight$^{0.33}$) was increased, and relative diastolic wall thickness was reduced in young (8-14 weeks) and/or old (50-67 weeks) mutants (Fig. 3E).

$Gja1^{Jrt}$/+ mutant mice crossed with FVB wild-type mice provided mutant offspring with sufficient body weight [although still 22% smaller as measured at 7 weeks (Fig. 4A)] to enable more detailed investigation of cardiac conduction deficits using chronic radio-telemetry implants. Ultrasound and histopathology analysis revealed no difference in $Gja1^{Jrt}$/+ × FVB mice relative to controls (not shown); however, conscious ambulatory ECGs (11-13 weeks) revealed a prolongation of the PQ interval, which is indicative of mild first degree AV block (Fig. 4A). In addition, P wave width was increased and the heart rate in $Gja1^{Jrt}$/+ × FVB mutants was lower than controls

(Fig. 4A). Several sporadic events were noted in $Gja1^{Jrt}$/+ × FVB mutants, including bradycardia, sinus pause with AV block, irregular sinus with AV dissociation and junctional escape, and a widened QRS complex (Fig. 4B). In the control group, only one mouse had notable events, namely bradycardia and 2nd degree AV block. It is possible these arrhythmias (Fig. 4A,B) were the cause of the premature death that we observed in 46 out of 170 $Gja1^{Jrt}$/+ mice (versus three out of 306 wild-type littermates).

Novel phenotypes of bone and hematopoietic stem cells in $Gja1^{Jrt}$/+ mutant mice

We also observed a number of phenotypes that have not been previously reported in individuals with ODDD, but which are consistent with known functions of Cx43. Bone mineral density (BMD), bone mineral content (BMC) and mechanical strength were all significantly reduced in $Gja1^{Jrt}$/+ × FVB mice versus wild-type littermates (+/+) at all ages tested (Fig. 5A; Table 1). Whole-mount Alcian Blue-Alizarin Red staining revealed that craniofacial bones originating from both mesoderm and neural crest cells displayed delayed
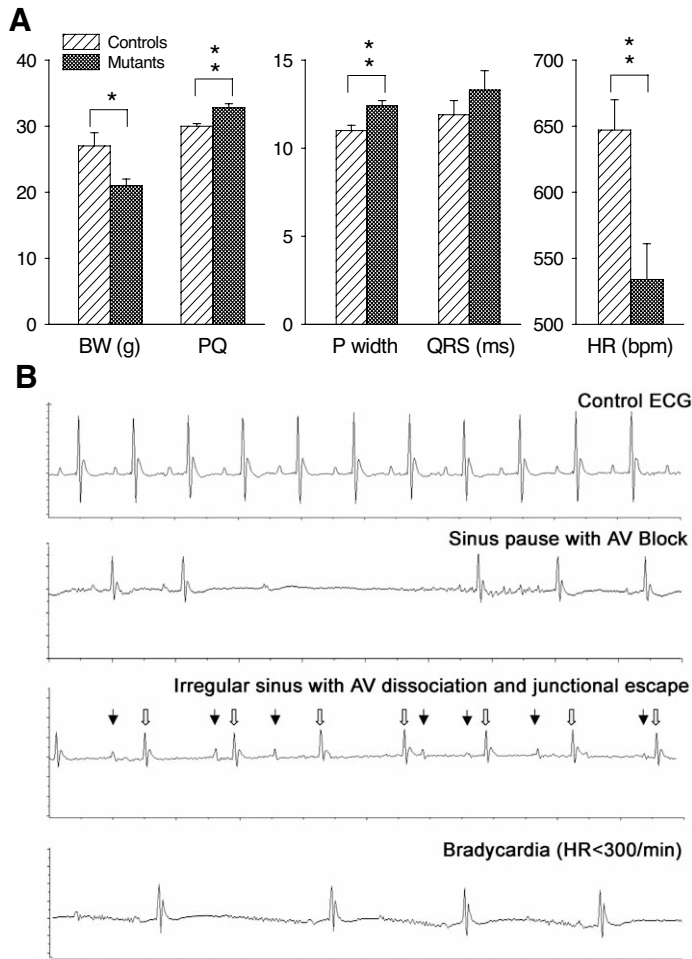
Fig. 4. ECG analysis of *Gja1^Jrt^/+* × FVB mutants by radio-telemetry. *Gja1^Jrt^/+* mutant mice crossed with FVB wild-type mice resulted in mice large enough to carry radio-telemetry implants for awake ECG analysis (A). Ultrasound (conducted at 7 weeks) and histopathology (conducted 10-12 weeks) analyses revealed no difference in *Gja1^Jrt^/+* × FVB mice relative to controls (not shown). However, conscious ambulatory ECGs (11-13 weeks) revealed a prolongation of the PQ interval indicative of mild first degree atrioventricular block (A). The PQ intervals were variable, occasionally increasing up to 43 mseconds in length. In addition, P wave width was increased and the heart rate (HR) in *Gja1^Jrt^/+* × FVB mutants was lower than controls. (B) Several sporadic events were noted in *Gja1^Jrt^/+* × FVB mutants: 5/9 had bradycardia (HR<300 minute^{-1}, with the lowest HR at 134 minute^{-1}), 4/9 had sinus arrest, 2/9 had widened QRS complex, 1/9 had AV block and 1/9 had AV dissociation and junctional escape. In the control group, only one mouse had notable events, namely bradycardia and 2nd degree AV block (not shown). *$P<0.05$, **$P\leqslant0.005$.

ossification, and were thin and porous with open foramena at 3 days and beyond, suggestive of an osteogenic defect (see Fig. S2 in the supplementary material). In adult mutant mice, all endochondral bones examined by micro-CT [femurs (Fig. 5B) and vertebrae (not shown)] and histological analysis [femurs (Fig. 5C), tibiae and sternebrae (not shown)] were osteopenic, but the phenotype was most marked in the long bones.

Although bone marrow atrophy (Fig. 5C) and associated bone marrow hypocellularity in conjunction with increased adipogenesis were apparent in young *Gja1^Jrt^/+* mutant mice (8 weeks) and progressed with age (17-51 weeks), peripheral blood counts were normal (data not shown), suggesting compensation by an increase in progenitors. In fact, the frequency of most mature hematopoietic lineages and their progenitors within the bone marrow were increased with the exception of erythroblasts (TER119+ cells; 3.3-fold decrease) and their progenitors (CFU-E; twofold decrease), which were decreased in total number and frequency (Fig. 6A and data not shown). Consistent with a role for Cx43 in regulating the stem cell niche, we found the bone marrow side population (SP) cells, a Hoechst-dye effluxing population enriched in hematopoietic stem cells and early progenitors (Goodell et al., 1996), was significantly increased in young (15 week) *Gja1^Jrt^/+* mice (2.4-fold increase; Fig. 6B) and further amplified with age (57-62 weeks) (3.5-fold increase; Fig. 6C).

## ODDD characteristics of variable penetrance not found in *Gja1^Jrt^/+* mutant mice

Additional symptoms with variable penetrance have been described in individuals with ODDD, including conductive hearing loss, and neurological dysfunction such as ataxia and paraparesis, along with changes in cerebral white matter and basal ganglia intensities on magnetic resonance imaging (MRI) (Loddenkemper et al., 2002). We did not detect any hearing abnormalities in five *Gja1^Jrt^/+* mutants at 10 weeks of age using the click box test. Although we have not undertaken an extensive neurological analysis in mutant mice, T2-weighted MRI analyses of the brains of *Gja1^Jrt^/+* mice (five mice, 52-60 weeks) did not show any variations in intensity compared with control wild-type mice (five mice, 52-60 weeks) (data not shown), nor did we detect weakness of the limbs or an abnormal gait as determined by prolonged observation and handling of the affected mice. More-sensitive neurological tests and/or testing at later ages may reveal more-subtle neurological deficits.

Localization and functional analysis of the *Gja1^Jrt^* mutant protein in vitro and in vivo

To assess whether Cx43^G60S^ could be transported to the cell surface and form gap junctions, we introduced an expression construct for a Cx43^G60S^-GFP tagged protein into both communication competent (NRK) and incompetent (HeLa, N2A) cells. In all cases, Cx43^G60S^-GFP was transported to the cell surface and assembled into gap junction-like structures (compare Fig. S3C,G,L with S3B,F,K in the supplementary material). However, the ability of Cx43^G60S^ to form functional gap junctions, as measured by dual patch clamp analysis, was severely affected. Only one out of 30 pairs of Cx43^G60S^ transfected N2A cells was coupled with a low level of junctional conductance (3.1 nS), compared with 31 out of 31 pairs of N2A cell pairs expressing wild-type Cx43, which were coupled with an average junctional conductance of 47±4.4 nS. This low percentage coupling (1/30) was not significantly different from non-transfected N2A cell pairs (data not shown).

To explore the effect of the *Gja1^Jrt^* mutation on gap junctional intercellular communication in cells from the mutant mice, we chose to examine ovarian granulosa cells. In granulosa cells of immature mouse ovarian follicles, Cx43 is

Fig. 5. Bone characteristics of *Gja1^{Jrt}*/+ mice. (A) Dual energy x-ray absorptiometry (PIXImus) to measure bone mineral content (BMC), bone area and bone mineral density (BMD) of femurs (males; 22 weeks) showed that BMC and BMD were significantly lower in *Gja1^{Jrt}*/+ × FVB mice compared with wild-type littermates (+/+). (B) The distal metaphysis of the left femurs were scanned by micro-CT. Two-dimensional images were used to generate 3D reconstructions that clearly showed reduced trabeculae and thin cortices in *Gja1^{Jrt}*/+ mice compared with wild-type littermates (+/+) at 12 weeks and 6 weeks (data not shown). Morphometric parameters, including percent bone, trabecular thickness distribution, trabecular connectivity, structure model index and cortical thickness, calculated with 3D Creator software supplied with the instrument confirmed the osteopenia in *Gja1^{Jrt}*/+ animals (not shown). (C) Hematoxylin and Eosin-stained paraffin sections of distal femurs in control (+/+) and in *Gja1^{Jrt}*/+ mice. A reduction in bone trabeculae was seen as early as 8 weeks of age in the *Gja1^{Jrt}*/+ mice versus the control mice (*i*), and progressive bone marrow atrophy was observed in *Gja1^{Jrt}*/+ mice at 17-18 weeks (*ii*) and 25 weeks (*iii*). With aging, the bone marrow space was almost completely atrophied in 51 week *Gja1^{Jrt}*/+ mice versus the 62 week control (+/+) (*iv*).
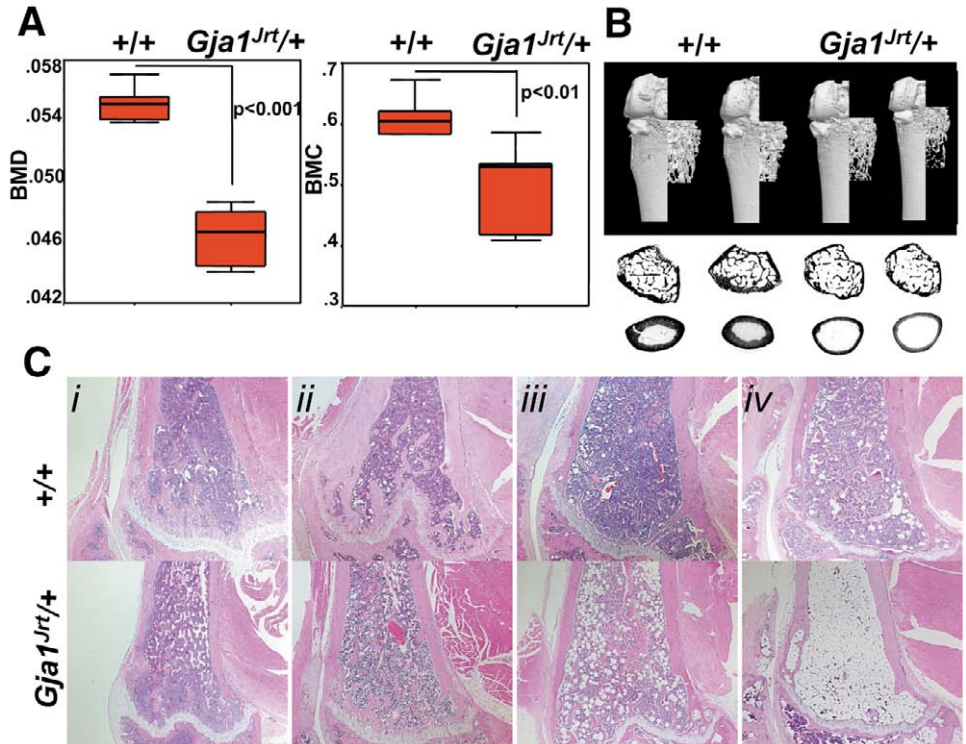
the sole connexin involved in cell-cell coupling, providing an ideal cell type to monitor Cx43 function in *Gja1^{Jrt}* mutants (Gittens et al., 2003; Veitch et al., 2004). In *Gja1^{Jrt}*/+ × FVB ovaries, only a few scattered gap junction plaques were seen when compared with wild-type cells (+/+) (Fig. 7A). This difference was maintained in granulosa cells growing out from follicles cultured in vitro (Fig. 7B), which were then tested for gap junctional coupling by Lucifer yellow dye injection (Fig. 7C-E) and by capacitative current transient analysis (Fig. 7F,G). Whereas all wild-type granulosa cells were strongly dye coupled, mutant cells were of two distinct types: those that were not detectably coupled (17 of the 27 cells tested) and those that were weakly coupled (10 out of 27; Fig. 7D). For those mutant granulosa cells that were coupled, the mean number of cells receiving dye from an injected cell was 2.2 when compared with 32.9 for wild-type cells (Fig. 7E), which was significantly different according to an unpaired *t*-test (*P*<

0.05). Analysis of the capacitative current transients obtained from granulosa cells of mutant follicles confirmed the existence of distinct populations of weakly coupled and non-coupled cells. In cultured wild-type follicles, the granulosa cells were well coupled, as indicated by large steady-state currents and slow decay phases in response to the voltage step (Fig. 7G). By contrast, the steady-state currents and decay phases from Cx43 knockout granulosa cells (*Gja1⁻/Gja1⁻*) (Fig. 7G) were indistinguishable from those of single completely isolated wild-type granulosa cells (not shown), confirming that the knockout granulosa cells were not electrically coupled. Whereas some (five out of 17) *Gja1^{Jrt}*/+ mutant granulosa cells were no better coupled than Cx43 knockout granulosa cells, the remaining 12 displayed a weak capacitative current, indicating the presence of limited gap junctional coupling (Fig. 7G). The difference in the strength of intercellular conductance between wild-type and coupled mutant cells (Fig. 7F) was significant (*P*<0.05) and similar to the difference in strength of coupling revealed by dye transfer (Fig. 7E). Thus, gap junctional coupling among mutant granulosa cells is both sporadic and weak, consistent with the paucity of gap junctions revealed by immunostaining.

Using western blot analysis, we quantified the steady state levels of total Cx43 protein (both normal and mutant) to determine if the presence of the mutant protein was affecting the 50% level of wild-type protein that should be present in the *Gja1^{Jrt}*/+ heterozygotes. We found a major reduction in total Cx43 protein and almost complete absence of the slower migrating phosphorylated species in mutant hearts and ovaries (Fig. 7H).
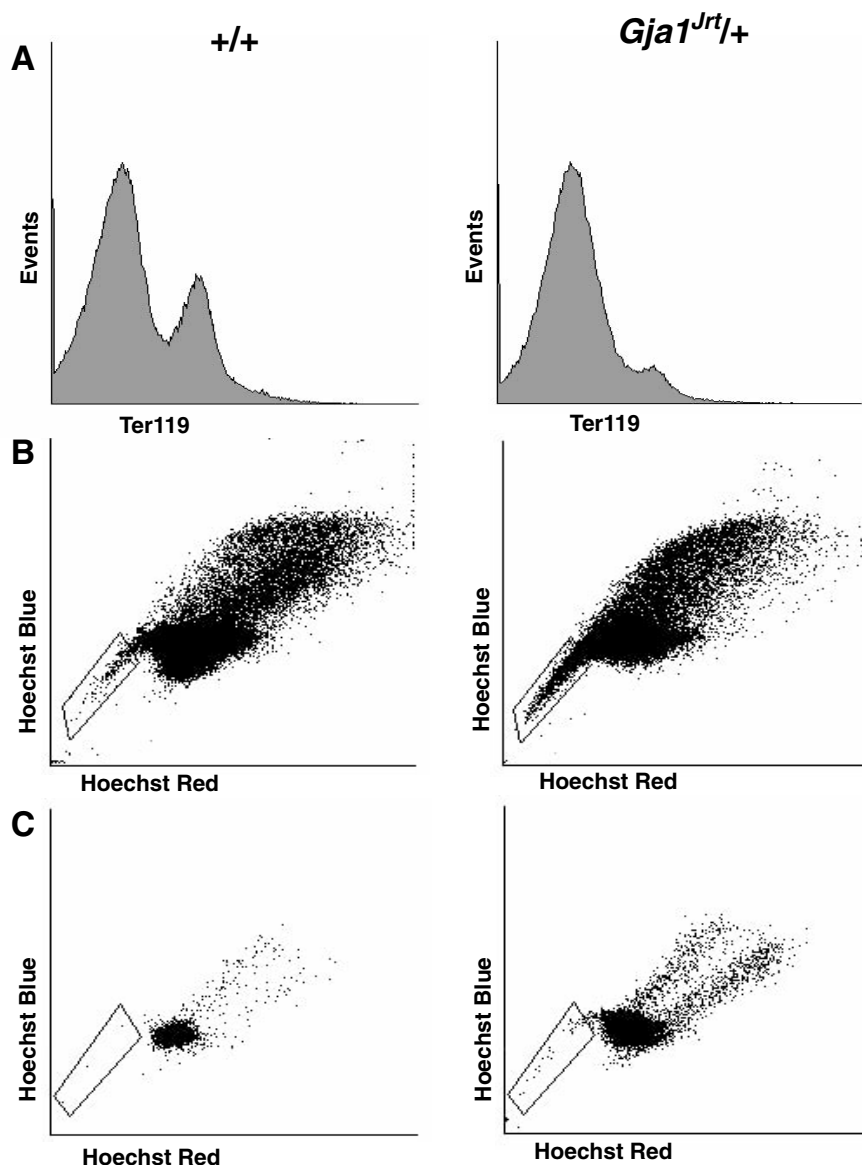
Table 1. Mechanical properties of *Gja1^{Jrt}*/+ × FVB bones

Bone mechanical test	+/+	*Gja1^{Jrt}*/+ × FVB
Ultimate load (N)	26.6	18.4 (*P*=0.01)
Toughness (mJ)	10.5	11.9 (*P*=0.59)
Stiffness (N/mm)	192.9	128.8 (*P*=0.004)
Failure displacement (mm)	0.56	0.94 (*P*=0.038)

Destructive three-point bending was performed on femurs of five *Gja1^{Jrt}*/+ × FVB mice and six wild-type littermates (males, age=22 weeks). Bones from *Gja1^{Jrt}*/+ × FVB mice have low resistance to load owing to low stiffness, and are weak and ductile. Although the toughness of *Gja1^{Jrt}*/+ × FVB and wild-type bones is similar, the toughness properties of mutant bones results in large plastic (permanent) deformation and at much lower loads.

Fig. 6. Flow cytometric analysis of affected bone marrow populations in *Gja1^Jrt*/+ mice. (A) TER119+ erythroblast population was dramatically diminished in affected *Gja1^Jrt*/+ mice compared with control littermates (+/+). (B,C) Gating of the side population (SP) of Hoechst dye effluxing cells from viable whole bone marrow, which are highly enriched in hematopoietic stem cells and primitive progenitors. (B) Young, 15-week-old and (C) 57-62 week old *Gja1^Jrt*/+ mice exhibit an amplified population of SP cells (indicated by box) compared with control littermates (+/+), suggesting increased stem and/or progenitor cells in the affected mice.

transmembrane domain (Yu et al., 2004). These findings suggest that the human *GJA1* mutations and the mouse *Gja1^Jrt* mutation, both of which result in ODDD in the heterozygous state, cannot be acting as simple loss-of-function mutations. Here, we have undertaken in vitro and in vivo experiments to determine the mechanism of action of the *Gja1^Jrt* (Cx43^G60S) mutation on normal gap junction function. Analysis of Cx43 localization and electrical coupling of transfected cells expressing Cx43^G60S-GFP showed that this mutation, although not preventing localization of the mutant connexin at the cell surface in gap junction plaque-like structures, is not compatible with the formation of functional intercellular membrane channels. Immunohistochemistry on ovarian and myocardial tissues revealed that Cx43 gap junction plaques were greatly reduced in *Gja1^Jrt*/+ mice when compared with control littermates. Further quantification of total Cx43 protein levels in ovary and heart tissue by western blot analysis confirmed that the reduction of Cx43 was far below 50%, indicating that the levels of normal Cx43 were also affected in the mutants. This low level of Cx43 protein corresponded to weak gap junctional coupling in granulosa cells growing out from cultured mutant follicles. Thus, both in vivo and in vitro evidence has revealed that *Gja1^Jrt*, and probably human ODDD mutations (Roscoe et al., 2005), are not simply loss-of-function mutations but rather function as dominant-negative mutations. The Cx43^G60S mutation is located in the first extracellular loop, a domain that has been shown to be crucial for the docking process (Foote et al., 1998). It is possible that this mutation impedes the formation of a functional intercellular channel by interfering with the ability of one hemichannel to dock with another hemichannel in an apposing cell. This inability to dock may result in the destabilization of channels that consist of a mixture of mutant and normal Cx43 and in the subsequent turnover of these proteins within the faulty hemichannel. Given the general absence of the more highly phosphorylated Cx43 species, we cannot eliminate the possibility that mixed oligomers of mutant

Discussion

Gja1^Jrt/+ mice have similar syndactlyly, enamel hypoplasia, cataract and iris abnormalities, and craniofacial dysplasia as individuals suffering from ODDD, making them the first in vivo model of this disease. The existence of these mice allowed us to examine gap junction histology and function in mutant tissues, which could not be undertaken in the human. To date 27 distinct missense, duplication and frameshift mutations in *GJA1* have been reported in individuals with ODDD (Kjaer et al., 2004; Paznekas et al., 2003; Richardson et al., 2004; van Steensel et al., 2005; Vitiello et al., 2005), including some within the same functional domain as this *Gja1^Jrt* (Cx43^G60S) mutation (Fig. 8).

In contrast to heterozygous *Gja1^Jrt*/+ mutants, mice heterozygous for a *Gja1*-null mutation showed no ODDD-like phenotypes (Houghton et al., 1999; Reaume et al., 1995), nor were ODDD characteristics reported for heterozygous mice resulting from an ENU-induced mutation in *Gja1* that generated a premature stop codon just after the first

Fig. 7. Immunostaining and intercellular coupling via gap junctions in primary granulosa cells. (A) Immunostaining for Cx43 (green) in granulosa cells in vivo and (B) in vitro showed only a few scattered gap junction-like plaques in $Gja1^{Jrt}/+ \times$ FVB granulosa cells. O, oocyte. Scale bars: 20 μm. (C,D) Lucifer dye injection (asterisks mark injected cells) revealed strong dye coupling among wild-type granulosa cells (+/+), whereas dye coupling among granulosa cells from cultured $Gja1^{Jrt}/+$ $\times$ FVB mutant follicles was severely restricted. O, oocyte. Scale bar: 50 μm. (E) Graphical representation of the mean number of neighboring cells receiving dye after injection where the number of cells tested is shown in parentheses above each bar. (F) The mean conductance of cells that were electrically coupled, as indicated by capacitative current transients, showed that coupling was severely reduced in $Gja1^{Jrt}/+ \times$ FVB granulosa cells. The number of cells tested is shown in parentheses above each bar. (G) Representative current transients from wild type (+/+), $Gja1$-null ($Gja1^-/Gja1^-$) and $Gja1^{Jrt}/+ \times$ FVB granulosa cells show that $Gja1^{Jrt}/+ \times$ FVB granulosa cells exhibited either very weak coupling or a complete lack of coupling (12/17 weakly coupled; 5/17 not coupled). In vivo and in vitro experiments were performed on primary granulosa cells isolated from ovaries on both genetic backgrounds with similar results. (H) Western blots reveal that the level of total Cx43 and especially the slower migrating phosphorylated species, was greatly reduced in heart and ovary from $Gja1^{Jrt}/+$ versus wild-type (+/+) mice (11 weeks). GAPDH was used as a gel loading control.
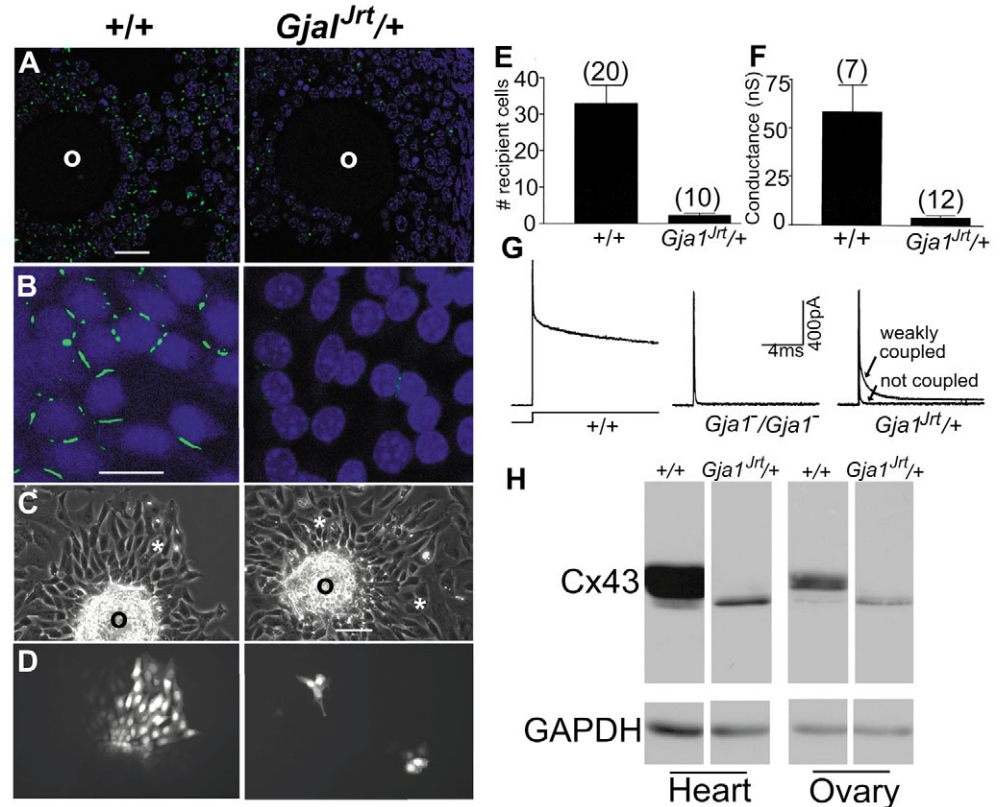
and wild-type Cx43 have impaired trafficking to the cell surface and are diverted into premature degradation pathways. Nevertheless our studies suggest that ubiquitous Cx43-mediated gap junctional intercellular communication would be sufficiently reduced in individuals with ODDD to result in the pleiotropic developmental defects and pathologies recapitulated in the $Gja1^{Jrt}/+$ mutant mouse. It is possible that the mutant Cx43 protein also perturbs interactions with other connexin (Saez et al., 2003) and non-connexin proteins (Giepmans, 2004) contributing to the complex ODDD phenotype.

Previous studies on Cx43-null mice and on $Gja1$ expression patterns in wild-type mice have emphasized the importance of gap junction function in normal development. Expression of $Gja1$ in the developing limb, craniofacial complex (Richardson et al., 2004) and teeth (Joao and Arana-Chavez, 2003) strongly correlates with tissues affected in ODDD. Cx43 is known to play a key role in electrical coupling between cardiomyocytes and in cardiac neural crest migration (Dhein, 1998; Lo et al., 1999). Cardiomyocyte-specific deletion of Cx43 or induced deletion of Cx43 in adult mice causes cardiac conduction defects and arrhythmias leading to early death (Eckardt et al., 2004; Gutstein et al., 2001), as observed here in the $Gja1^{Jrt}/+$ mutants. Heterozygous Cx43-null embryos have enlargement of the RV chamber accompanied by thinning of the chamber wall (Huang et al., 1998b), whereas Cx43-null mutants die at

birth owing to RV outflow tract obstruction (Reaume et al., 1995) resulting from abnormal migration of cardiac neural crest (Huang et al., 1998a). As in individuals with ODDD, however, the RV outflow tract in $Gja1^{Jrt}/+$ mutants was apparently normal (pulmonary artery dimensions and pulmonary artery Doppler velocities were normal) as were the RV chamber dimension and RV wall thickness in younger mutants. Thus, the reduction in Cx43 function in $Gja1^{Jrt}/+$ mutants seems to be more crucial for cardiac electrophysiological function than neural crest migration.

While examining the pleiotropic phenotypes presented by $Gja1^{Jrt}/+$ mice, we found additional abnormalities in osteogenesis and hematopoiesis that are consistent with known functions of Cx43. Craniofacial abnormalities with delayed ossification throughout the skeleton, but essentially normal appendicular and axial skeletons at birth, have previously been reported in homozygous Cx43-null mice (Lecanda et al., 2000). We also found delayed ossification in craniofacial bones, which may be the origin of the craniofacial abnormalities detected by micro-CT in older $Gja1^{Jrt}/+$ mice. Neonatal lethality precluded determination of whether the absence of Cx43 results in the reduced bone mass and mechanical strength in adult animals as observed in our $Gja1^{Jrt}/+$ mutant mice, although this might be predicted based on the osteoblast dysfunction observed in homozygous Cx43-null calvarial cells in vitro (Lecanda et al., 2000). Thus far,
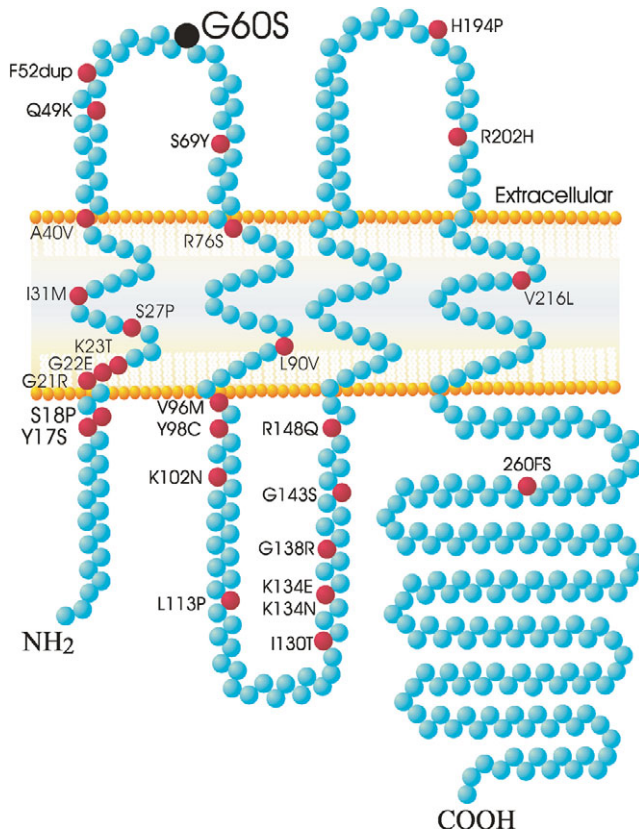
Fig. 8. Illustration of Cx43 protein structure showing known human ODDD mutations. Known human mutations resulting in ODDD (Kjaer et al., 2004; Paznekas et al., 2003; Richardson et al., 2004; van Steensel et al., 2005; Vitiello et al., 2005) are highlighted in red with the *Gja1^Jrt* mutation (G60S) highlighted in black. Missense mutations are denoted by the correct amino acid followed by the number and the substituted amino acid. The duplication (dup) and frameshift (FS) mutations are indicated by amino acid number followed by dup and FS, respectively.

bone mineralization defects have not been reported in humans with ODDD; however, these results suggest that individuals should be examined for osteopenia, as it may pose a serious health risk for them, especially as they age.

Analyses of *Gja1*-null embryos and neonates have previously demonstrated a role for Cx43 gap junctions in the establishment of bone marrow hematopoiesis and lymphoid maturation (Cancelas et al., 2000; Krenacs et al., 1997). The role of stromal Cx43 gap junctions in the bone marrow stem cell niche and in adult hematopoiesis, however, could not be addressed as Cx43 null neonates die shortly after birth. Adult *Gja1^Jrt*/+ mutant mice had normal peripheral blood counts despite having bone marrow atrophy, which is probably due to a concomitant increase in mature hematopoietic lineages and their progenitors within the bone marrow, possibly owing to the enrichment in hematopoietic stem cells and early progenitors. These findings reveal a crucial role for stromal gap junctions in adult steady-state hematopoiesis in addition to developmental hematopoiesis. No human hematological abnormalities have been reported in individuals with ODDD, although this may be due to the complex homeostatic

mechanisms that regulate this tissue. Over the lifetime of an individual, homeostatic regulation often breaks down, suggesting that blood abnormalities may develop in older individuals with ODDD.

The *Gja1^Jrt*/+ mice did not display a subset of the variably penetrant symptoms of ODDD, including conductive hearing loss and neurological disorders such as weakness of the lower extremities and abnormal gait. Although it may be necessary to perform more sensitive neurological tests to reveal subtle neurological deficits, it is also possible that mutations in specific domains of the Cx43 protein generate a variable spectrum of phenotypes as different domains are known to govern diverse properties of the gap junction channel such as conductance, permeability and protein interactions. Importantly, this animal model of ODDD allows for a thorough evaluation of Cx43 function under conditions where both the wild-type and mutant Cx43 are predicted to be expressed at equal levels. In addition, these mice provide new insights into potential defects or abnormalities that may have remained undetected or undiagnosed in individuals with ODDD, and, in future, will provide a useful model with which to develop and evaluate potential intervention strategies for the treatment of ODDD.

Supplementary material

Supplementary material for this article is available at http://dev.biologists.org/cgi/content/full/132/19/4375/DC1

References

Broberg, C. S., Pantely, G. A., Barber, B. J., Mack, G. K., Lee, K., Thigpen, T., Davis, L. E., Sahn, D. and Hohimer, A. R. (2003). Validation of the myocardial performance index by echocardiography in mice: a noninvasive measure of left ventricular function. *J. Am. Soc. Echocardiog.* **16**, 814-823.

Cancelas, J. A., Koevoet, W. L. M., de Konig, A. E., Mayen, A. E. M., Rombouts, E. J. C. and Ploemacher, R. E. (2000). Connexin43 gap junctions are involved in multiconnexin-expressing stromal support of hemopoietic progenitors and stem cells. *Blood* **96**, 498-505.

de Roos, A. D., van Zoelen, E. J. and Theuvenet, A. P. (1996). Determination of gap junctional intercellular communication by capacitance measurements. *Pflugers Arch.* **431**, 556-563.

Dhein, S. (1998). Gap junction channels in the cardiovascular system: pharmacological and physiological modulation. *Trends Pharmacol. Sci.* **19**, 229-241.

Eckardt, D., Theis, M., Degen, J., Ott, T., van Rijen, H. V., Kirchhoff, S., Kim, J. S., de Bakker, J. M. and Willecke, K. (2004). Functional role of

connexin43 gap junction channels in adult mouse heart assessed by inducible gene deletion. *J. Mol. Cell Cardiol.* **36**, 101-110.

Foote, C. I., Zhou, L., Zhu, X. and Nicholson, B. J. (1998). The pattern of disulfide linkages in the extracellular loop regions of connexin32 suggests a model for the docking interface of gap junctions. *J. Cell Biol.* **140**, 1187-1197.

Gaser, C., Volz, H.-P., Kiebel, S., Riehemann, S. and Sauer, H. (1999). Detecting structural changes in whole brain based on nonlinear deformation-application to schizophrenia research. *NeuroImage* **10**, 107-113.

Giepmans, B. N. (2004). Gap junctions and connexin-interacting proteins. *Cardiovasc. Res.* **62**, 233-245.

Gittens, J. E. I., Mhawi, A. A., Lidington, D., Ouellette, Y. and Kidder, G. M. (2003). Functional analysis of gap junctions in ovarian granulosa cells: a distinct role for connexin43 in early stages of folliculogenesis. *Am. J. Physiol. Cell Physiol.* **284**, C880-C887.

Goodell, M. A., Brose, K., Paradis, G., Conner, A. S. and Mulligan, R. C. (1996). Isolation and functional properties of murine hematopoietic stem cells that are replicating in vivo. *J. Exp. Med.* **183**, 1797-1806.

Gutstein, D. E., Morley, G. E., Tamaddon, H., Vaidya, D., Schneider, M. D., Chen, J., Chein, K. R., Stuhlmann, H. and Fishman, G. I. (2001). Conduction slowing and sudden arrhythmic death in mice with cardiac-restricted inactivation of connexin43. *Circ. Res.* **88**, 333-339.

Holmes, A. P., Blair, m. C., Watson, G. J. D. and Ford, I. (1996). Nonparametric analysis of statistic images from functional mapping experiments. *J. Cereb. Blood Flow Met.* **16**, 7-22.

Houghton, F. D., Thonnissen, E., Kidder, G. M., Naus, C. C. G., Willecke, K. and Winterhager, E. (1999). Doubly mutant mice, deficient in Connexin32 and -43, show normal prenatal development of organs where the two gap junction proteins are expressed in the same cells. *Dev. Genet.* **24**, 5-12.

Huang, G. Y., Cooper, E. S., Waldo, K., Kirby, M. L., Gilula, N. B. and Lo, C. W. (1998a). Gap junction mediated cell-cell communication modulates mouse neural crest migration. *J. Cell Biol.* **143**, 1725-1734.

Huang, G. Y., Wessels, A., Smith, B. R., Linask, K. K., Ewart, J. L. and Lo, C. W. (1998b). Alteration in connexin 43 gap junction gene dosage impairs conotruncal heart development. *Dev. Biol.* **198**, 32-44.

Ito, C. Y., Li, C. Y. J., Bernstein, A., Dick, J. E. and Stanford, W. L. (2003). Hematopoietic stem cell and progenitor defects in Sca-1/Ly-6A null mice. *Blood* **101**, 517-523.

Joao, S. M. A. and Arana-Chavez, V. E. (2003). Expression of connexin43 and ZO-1 in differentiating ameloblasts and odontoblasts from rat molar tooth germs. *Histochem. Cell. Biol.* **119**, 21-26.

Justice, M. J., Carpenter, D. A., Favor, J., Neuhauser-Klaus, A., Hrabe de Angelis, M., Soewarto, D., Moser, A., Cordes, S., Miller, D., Chapman, V. et al. (2000). Effects of ENU dosage on mouse strains. *Mammal. Genome* **11**, 484-488.

Kjaer, K. W., Hansen, L., Eiberg, H., Leicht, P., Opitz, J. M. and Tommerup, N. (2004). Novel connexin43 (GJA1) mutation causes oculo-dento-digital dysplasia with curly hair. *Am. J. Med. Genet.* **127A**, 152-157.

Kovacevic, N., Henderson, J. T., Chan, E., Lifshitz, N., Bishop, J., Evans, A. C., Henkelman, R. M. and Chen, X. J. (2005). A three-dimensional MRI atlas of the mouse brain with estimates of the average and variability. *Cereb. Cortex* **15**, 639-645.

Krenacs, T., van Dartel, M., Lindhout, E. and Rosendaal, M. (1997). Direct cell/cell communication in the lymphoid germinal center: connexin43 gap junctions functionally couple follicular dendritic cells to each other and to B lymphocytes. *Eur. J. Immunol.* **27**, 1489-1497.

Laird, D. W., Castillo, M. and Kasprzak, L. (1995). Gap junction turnover, intracellular trafficking and phosphorylation of connexin43 in brefeldin A-treated rat mammary tumor cells. *J. Cell Biol.* **131**, 1193-1203.

Lecanda, F., Warlow, P. M., Sheikh, S., Furlan, F., Steinberg, T. H. and Civitelli, R. (2000). Connexin43 deficiency causes delayed ossification, craniofacial abnormalities, and osteoblast dysfunction. *J. Cell Biol.* **151**, 931-943.

Lo, C. W., Waldo, K. L. and Kirby, M. L. (1999). Gap junction communication and the modulation of cardiac neural crest cells. *Trends Cardiovasc. Med.* **9**, 63-69.

Loddenkemper, T., Grote, K., Evers, S., Oelerich, M. and Stogbauer, F. (2002). Neurological manifestations of the oculodentodigital dysplasia syndrome. *J. Neurol.* **249**, 584-595.

McLeod, M. J. (1980). Differential staining of cartilage and bone in whole mouse fetuses by alcian blue and alizarin red S. *Teratology* **22**, 299-301.

Mitchell, J. A., Ting, T. C., Wong, S., Mitchell, B. F. and Lye, S. J. (2003). Parathyroid hormone-related protein treatment of pregnant rats delays the increase in connexin43 and oxytocin receptor expression in the myometrium. *Biol. Reprod.* **69**, 556-562.

Nieman, B. J., Bock, N. A., Bishop, J., Sled, J. G., Chen, X. J. and Henkelman, R. M. (2004). Fast spin-echo for multiple mouse MR phenotyping. *Magn. Reson. Med.* (in press).

Paznekas, W. A., Boyadjiev, S. A., Shapiro, R. E., Daniels, O., Wollnik, B., Keegan, C. E., Innis, J. W., Dinulos, M. B., Christian, C., Hannibal, M. C. et al. (2003). Connexin43 (GJA1) mutations cause the pleiotropic phenotype of oculodentodigital dysplasia. *Am. J. Hum. Genet.* **72**, 408-418.

Reaume, A. G., de Sousa, P. A., Kulkarni, S., Langille, B. L., Zhu, D., Davies, T. C., Juneja, S. C., Kidder, G. M. and Rossant, J. (1995). Cardiac malformation in neonatal mice lacking connexin43. *Science* **267**, 1831-1834.

Richardson, R. R., Donnai, D., Meire, F. and Dixon, M. J. (2004). Expression of Gja1 correlates with the phenotype observed in oculodentodigital syndrome/type III syndactyly. *J. Med. Genet.* **41**, 60-67.

Rogers, D. C., Fisher, E. M., Brown, S. D., Peters, J., Hunter, A. J. and Martin, J. E. (1997). Behavioral and functional analysis of mouse phenotype: SHIRPA, a proposed protocol for comprehensive phenotype assessment. *Mammal. Genome* **8**, 711-713.

Roscoe, W. A., Barr, K. J., Mhawi, A. A., Pomerantz, D. K. and Kidder, G. M. (2001). Failure of spermatogenesis in mice lacking connexin43. *Biol. Reprod.* **65**, 829-838.

Roscoe, W. A., Veitch, G. I., Gong, X. Q., Pellegrino, E., Bai, D., McLachlan, E., Shao, Q., Kidder, G. M. and Laird, D. W. (2005). Oculodentodigital dysplasia-causing connexin43 mutants are non-funtional and exhibit dominant effects on wild-type connexin43. *J. Biol. Chem.* **280**, 11458-11466.

Saez, J. C., Berthoud, V. M., Branes, M. C., Martinez, A. D. and Beyer, E. C. (2003). Plasma membrane channels formed by connexins: their regulation and functions. *Physiol. Rev.* **83**, 1359-1400.

Sohl, G. and Willecke, K. (2004). Gap junctions and the connexin protein family. *Cardio. Res.* **62**, 228-232.

Thomas, T., Telford, D. and Laird, D. W. (2004). Functional domain mapping and selective trans-dominant effects exhibited by Cx26 disease-causing mutations. *J. Biol. Chem.* **279**, 19157-19168.

Valverde-Franco, G., Liu, H., Davidson, D., Chai, S., Valderrama-Carvajal, H., Goltzman, D., Ornitz, D. M. and Henderson, J. E. (2004). Defective bone mineralization and osteopenia in young adult FGFR3–/– mice. *Hum. Mol. Gen.* **13**, 271-284.

van Steensel, M. A. M., Spruijt, L., van der Burgt, I., Bladergroen, R. S., Vermeer, M., Steijlen, P. M. and van Geel, M. (2005). A 2-bp deletion in the GJA1 gene is associated with oculo-dento-digital dysplasia with palmoplantar keratoderma. *Am. J. Med. Genet.* **132A**, 171-174.

Veitch, G. I., Gittens, J. E. I., Shao, Q., Laird, D. W. and Kidder, G. M. (2004). Selective assembly of connexin37 into heterocellular gap junctions at the oocyte/granulosa cell interface. *J. Cell Sci.* **117**, 2699-2707.

Vitiello, C., D'Adamo, P., Gentile, F., Vingolo, E. M., Gasparini, P. and Banfi, S. (2005). A novel GJA1 mutation causes Oculodentodigital Dysplasia without Syndactyly. *Am. J. Med. Genet.* **133A**, 58-60.

Yu, Q., Shen, Y., Chatterjee, B., Seigfried, B. H., Leatherbury, L., Rosenthal, J., Lucas, J. F., Wessels, A., Spurney, C. R., Wu, Y.-J. et al. (2004). ENU induced mutations causing congenital cardiovascular anomalies. *Development* **131**, 6211-6223.

Zhou, Y. Q., Foster, F. S., Neiman, B. J., Davidson, L., Chen, X. J. and Henkelman, R. M. (2004). Comprehensive transthoracic cardiac imaging in mice using ultrasound biomicroscopy with anatomical confirmation by magnetic resonance imaging. *Physiol. Genomics* **18**, 232-244.